Spring 2023

Experimental Determination of Zinc, Potassium and Rubidium Diffusion Coefficients in Olivine

Christopher J. Willingham
Missouri State University, Willingham787@live.missouristate.edu

EXPERIMENTAL DETERMINATION OF ZINC, POTASSIUM AND RUBIDIUM DIFFUSION COEFFICIENTS IN OLIVINE

A Master's Thesis

Presented to

The Graduate College of

Missouri State University

In Partial Fulfillment

Of the Requirements for the Degree

Master of Science, Geography and Geology

By

Christopher Willingham

May 2023

EXPERIMENTAL DETERMINATION OF ZINC, POTASSIUM AND RUBIDIUM DIFFUSION COEFFICIENTS IN OLIVINE

Geography, Geology, and Planning

Missouri State University, May 2023

Master of Science

Christopher Willingham

ABSTRACT

One of NASA's key strategies is to learn more about the early solar system and its formation. Chondrites were formed from the most primitive materials at the collapse of the solar system and over time have been classified into different categories based on their elemental abundance. These chondrites have fallen to Earth and have even formed entities such as asteroids and planetary bodies. It has been found through studies that one of these chondrites is close to the elemental abundance of the Sun. The other types of chondrites were up to two orders of magnitude less in concentration compared to the Sun's photosphere. The question arises to why these chondrites are less in concentration. Our hypothesis is that diffusion may play a role in this difference. In order to check this hypothesis, an experiment was created using a Knudsen Effusion Cell chamber in which the atmosphere would be lowered to close to 1×10^{-8} torr which would keep the oxygen fugacity lower than that level. The temperatures for this study would be between 1300 and 1800 degrees Celsius. The material used for these experiments would be the standards of BHVO-2, a Hawaiian basalt, and a San Carlos olivine. The purpose is to show that at these temperatures the elements being analyzed, Zinc, Potassium, and Rubidium, will diffuse from the basalt into the crystal. After the experiment, it was found that the elements didn't diffuse, but volatilized and left the system. Each of the elements lost up to ninety percent of their concentration even from the olivine crystal.

KEYWORDS: olivine, Rubidium, Potassium, Zinc, diffusion, basalt, experimental, petrology, chondrites

EXPERIMENTAL DETERMINATION OF ZINC, POTASSIUM AND RUBIDIUM DIFFUSION COEFFICIENTS IN OLIVINE

By

Christopher Willingham

A Master's Thesis
Submitted to the Graduate College
Of Missouri State University
In Partial Fulfillment of the Requirements
For the Degree of Master of Science, Geography and Geology

May 2023

Approved:

Gary Michelfelder, Ph.D., Thesis Committee Chair

David Cornelison, Ph.D., Committee Member

Kevin Mickus, Ph.D., Committee Member

Julie Masterson, Ph.D., Dean of the Graduate College

ACKNOWLEDGEMENTS

Hello there! I would like to thank the following people for their support during my graduate studies. First, I would like to thank NASA, Missouri Space Grant Consortium, and the Missouri State Graduate College for making this research possible. I would like to thank Dr. Gary Michelfelder for guiding me through this process. I would also like to thank Dr. David Cornelison for presenting the opportunity to work on this project and to be on my committee. I would also like to thank Dr. Kevin Mickus for serving on the committee. A special thank you to Dr. Barry Shaulis for assisting with trace element analysis using the LA-ICP-MS at the University of Arkansas. Finally, I would like to thank the following graduate students for their support throughout my graduate experience: Caesar Bucheli, Sarah Rasor, Nathan Lenhard, Bennet Van Horn, Joe Lane, and Trevor Sanders. Thank you to all the undergraduate and graduate students on the third floor to make the experience fun. Thank you to all the professors for their time and knowledge in and out of classes.

TABLE OF CONTENTS

LIST OF TABLES

LIST OF FIGURES

INTRODUCTION

The formation of the early solar system and the planetary bodies led to the depletion of elements compared to the bulk solar composition (i.e., CI chondrites). The depletion is most apparent in the moderately volatile elements (MVE) and volatile elements (VE) where at least one order of magnitude depletion has occurred between planetary bodies and CI chondrites (Neumann et al. 2022). Additionally, the MVE and VE compositions differ in magnitude of depletion from the differences observed in isotopic fractionation leading to ambiguity in explaining a mechanism for depletion and have not been explained by a specific mechanism for elemental fractionation.

Phase transformation from solid or liquid to a gas is a ubiquitous process in geologic materials and commonly observed during degassing of magmatic systems and during impact events, and on a larger scale during planetary accretion during the formation of planetary bodies (Sossa et al. 2019). During early solar system formation, the volatility of an element is determined by the temperature which 50% of the mass is condensed at equilibrium, or the **"**50% condensation temperature (T_c^{50})**"** (Larimer 1967). Volatile and moderately volatile elements are those elements which have a T_c^{50} less than 704K and 1290K, respectively, and therefore, make then useful in understanding the formation of the solar system. Chondrite normalized abundances of MVE**'**s in planetary bodies versus T_c^{50} defines the volatility trends of an element for rocky planetary bodies. The depletion of the elements suggests further depletion in the mantles and cores of these bodies (e.g., Wood et al. 2006; Siebert and Shahar 2015;). Essentially, the depletion of these elements reflects the complex nature of planetary formation starting from dust to the differentiation of planetary bodies from thermal events. Multiple models have been suggested to explain this depletion ranging from formation from

volatile-poor lunar dust to thermal fractionation during protoplanet development, and even outgassing during the existence of magma oceans (Bourdon and Fitousi 2020). The common factor in all these models is in the necessary phase transition between a solid to a gas phase for MVEs. This transition is commonly simplified in the most experimental determination of MVE fractionation where only a gas and liquid composition are considered (Neumann et al. 2022). Distinguishing between these processes adds complexity to experiments but in a nontrivial factor.

Potassium (K), rubidium (Rb), and zinc (Zn) are particularly well suited to investigate MVE fractionation between a solid (or liquid) and the evaporation gas phase and tracing the origin of MVE depletion in the solar system due to their low T_c[50], similar chemical behavior when partitioning into solid phases, and abundances in basaltic composition rocks (Zhang et al. 2021). Here, this study presents the results of experiments conducted at vacuum and high temperatures like those calculated during early solar system formation to determine the effect of a solid phase inhibiting or enhancing MVE fractionation. The objectives of the study are to (1) determine the evaporation kinetics of K, Rb, and Zn in a basalt which contains a solid phase in thermal equilibrium; (2) determine the diffusion properties of these elements between the solid and the liquid during evaporation; and (3) determine if evaporation enhances diffusion of MVE between the solid and liquid phases. I present the experimental results of MVE and trace element behavior/loss from a solid phase during evaporation of a basalt liquid. By providing analysis of Zn, Rb, and K along with non-volatile elements, we can provide a framework for interpreting data from natural samples where experimental data may be lacking.

BACKGROUND

A key strategic mission of NASA is understanding more about the early solar system and its formation. Upon the collapse of the solar nebular, elements and molecules were vaporized resulting from a major heating event. Within minutes, these vapors started to condense and accrete to form astronomical bodies such as meteorites, asteroids, and planetesimal bodies. Meteorites and asteroids have been the focus of study to understand these events, leading to a classification based on representation in the early solar system (Prior 1920). Carbonaceous chondrites were named this way due to their high amount of carbon (Anders et al. 1982). These were determined to be like elemental abundance estimates except for volatile elements such as carbon, hydrogen, oxygen nitrogen, and noble gases (Anders 1989). As a result, moderately volatile elements (MVE) were selected to further study these chondrites (Figure 1).

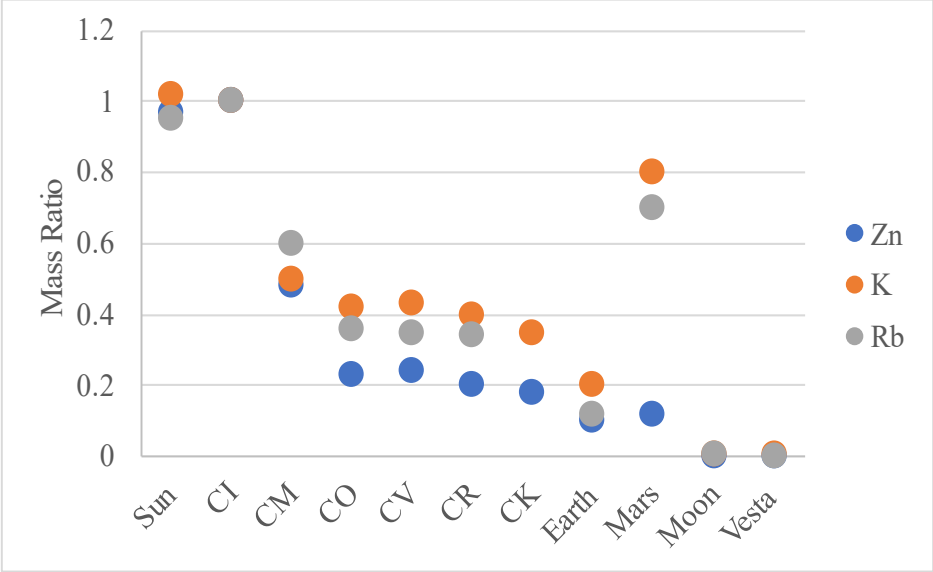

Figure 1. The carbonaceous chondrite and planetary bodies mass ratios for Zn, K, and Rb (Bloom et al., 2020).

MVEs are elements which have T_c^{50} temperature between 650K and 1250K (Lodders 2003). They include elements such as lithium (Li), sodium (Na), chlorine (Cl), potassium (K), copper (Cu), zinc (Zn), and rubidium (Rb); (Lodders 2003). Previous studies suggest primitive bodies of the solar system are enriched in MVEs, whereas bodies such as the Moon and Earth have become depleted (Palme et al. 1988). This study may help in determining how MVEs respond to certain mechanisms which in turn would help learn more about planet building for future studies (Mahan et al. 2018). The behavior of these elements during melting, evaporation and condensation depends on the resident thermodynamic conditions, and exploring this variable can shed light on prevailing conditions during chondrule formation and recycling and may also provide information on delivery of water (Mahan et al. 2018).

Potassium has a nebular condensation temperature Tc50 of 1006K. Potassium informs on the radiogenic heat production, atmospheric composition and volatile element depletion of the Earth and other planetary system (Farcy et al. 2020). Many planetary bodies show variable depletion in potassium, often quantified by the K/U ratio (Ku et al. 2020). Secondary analysis of potassium depletion can be passed through the Copper (Cu)/K ratio because Calcium (Ca) is a refractory major element, with well-defined and relatively constant concentrations (Ku et al. 2020). It has also been found that K-isotopic composition of bulk silicate Mars (BSM) and the strong correlation between δ41K and planet mass reveals that the sizes of planetary bodies fundamentally control their ability to retain volatiles (Tian et al. 2020).

Rubidium has a nebular condensation temperature T_c^{50} of 800K. It is the most volatile of the three elements of study in this study, and it provides an alternative alkali-metal isotope tracer for high-temperature processes in cosmochemistry (O'Neill and Palme 2008). In bulk chondrites, the present amount of Rb is roughly 1-2 ppm (Lodders et al. 1998), and bonds with similar

strengths to K (Zeng et al. 2019). It, along with K, are strong lithophile elements (Norris and Wood 2017; Tera et al. 1970) and is highly incompatible, which makes it enriched in highly differentiated terrestrial rocks such as pegmatites (McKenzie et al 1991; Beattie et al. 1993). Rubidium is an element that due to its apparent depletion in the BSE compared to chondrites, its moderately volatile nature, and its importance for the Rb-Sr isotope system is ideally suited to investigate the fate of volatile elements in the BSE (Nebel et al. 2011). Nebel et al. (2011) suggest that Rb could be an excellent tracer for Pb since their T_c^{50} are roughly the same (800K to 727K). The variations in Rb isotope compositions in the volatile-poor samples are attributed to volatile loss from planetesimals during accretion. Due to the similar incompatibility of Rb and Sr, the Rb/Sr ratio is generally constant in planetary materials and is a useful indicator of volatile depletion since Sr (T_c = 1455K) is much more refractory than Rb (Pringle et al. 2017)

Zinc (Zn) has many qualities that lend itself to being a primary element of interest in this study. First, Zn is a moderately volatile element and has a T_c^{50} of 726K. Second, its characteristics behave mainly as a lithophile element during planetary differentiation, due to 70% of Zn outside of the Earth's core and slightly siderophile due to roughly 30% of terrestrial Zn being stored in the Earth's core (Moynier et al. 2017). Zinc also has five different isotopes, but three are abundant enough to be studied properly: ^{64}Zn (48.6%), ^{66}Zn (27.9%) and ^{68}Zn (18.8%). The isotopes of Zn are being used to investigate volatile loss, igneous fractionation, and to understand mechanisms that are associated with core formation processes (Chen et al. 2013).

Zinc has been used as a proxy for MVE fractionation. It is used to measure fractionation in astronomical bodies (Luck et al. 2005; Moynier et al. 2011; Pringle et al. 2017). One advantage of Zn isotopes is that the existence of more than two stable isotopes allows for fractionation during measurement to be more easily determined, which used terrestrial basaltic and ultramafic samples to define BSE δ^{66}Zn values at 0.28 ± 0.05‰ (Chen et al. 2013).

Investigation of Zn isotope behavior during magmatic differentiation through analysis of oceanic basalts and peridotites concluded that there is a small isotopic fractionation of 0.01‰ during mantle partial melting (Wang and Jacobson 2016; Huang et al. 2018). Later work on peridotites and komatiites provides a restricted range for Earth's Zn isotopic values of 0.16 ± 0.06‰ (Sossi et al. 2018). Both Zn isotope values of Earth turn out to be depleted compared to the 1.31 ± 0.13‰ average for the Moon (Paniello et al. 2012; Kato and Moynier 2017). Zinc is abundant enough in most planetary materials (typically>1ppm) so that it is possible to analyze its high-precision isotopic composition by processing less than 1 g of material (Dhaliwal et al. 2018). There is now a large high-precision dataset available for Zn isotope ratios and abundances of lunar samples (Moynier et al. 2006; Herzog et al. 2009; Paniello et al. 2012; Kato et al. 2015). Second, Zn isotopic compositions and abundances for lunar samples are typically reported from homogenized bulk rock aliquots, allowing for comparisons across different sample sets and lithologies (Dhaliwal et al. 2018), and since Zn is also not generally affected by strong partitioning into Zn-rich phases, except for sphalerite in some exceptional lunar samples (Shearer et al. 2014). The Zn measurements differ from those of chlorine, which can be measured in situ in lunar apatite grains (Sharp et al. 2010) and sulfur, which is observed in sulfides differentiation signatures that could persist in the lunar mantle (Labidi et al. 2013). Therefore, while the Zn data is limited to mostly bulk rock, it provides an important baseline for the behavior of volatile elements in planetary bodies but avoids issues of lunar post-crystallization alteration processes, which modify more volatile elements and compounds (Shearer et al. 2006). Third, Zn isotope compositions are not affected by secondary effects, such as solar wind spallation or cosmogenic effects (as is the case for the D/H ratio; Greenwood et al. 2011). Additionally, Zn does not experience significant isotopic fractionation during magmatic differentiation (Chen et al. 2013). For these reasons, studies have focused on

using the available Zn isotope data for lunar samples to examine models for volatile element loss during magma ocean processes, but the models may also be applicable to other volatile elements and MVE (Dhaliwal et al. 2018).

EXPERIMENTAL TECHNIQUES

The study presents an extension of the study by Neumann et al (2022) designed to determine MVE fractionation between liquid and gas states. One variable not constrained was the presence of a solid phase containing MVEs. The experiments have been redesigned to test this variable while extending the number of elements investigated. The new experiments consist of placing a single olivine crystal into a crucible filled with silicate melt. Experiments were conducted using a custom designed Knudsen Effusion Cell at Missouri State University.

Starting Materials

The San Carlos olivine (SC) was used as the solid crystalline material in this experiment and is a known geologic reference material (Spandler and O'Neill 2010; Lambart et al 2022). The material is a high-forsterite olivine (Fo_{88-92}),.and Zn concentration ranging from 50-56 ppm. Individual crystals were taken to a lab where they were cut with a diamond saw to a three-millimeter by three-millimeter by three-millimeter cube.

The Hawaiian basalt, BHVO-2 (Raczek et al. 2001), was selected as the silicate liquid in this experiment and is a known geologic reference (Table 1). The basalt powder surrounded the crystal in the crucible. The crucible is made of tantalum and has a cap and a body. A 0.0078 in. hole was drilled in the top of the crucible to allow for effusion in which the diameter is 0.1981 millimeters. The complete length of the crucible was 21.59 millimeters and was mounted on a molybdenum rod (Figure 2). The crystal will be placed on a bed of the basalt and then surrounded and covered by the basalt.

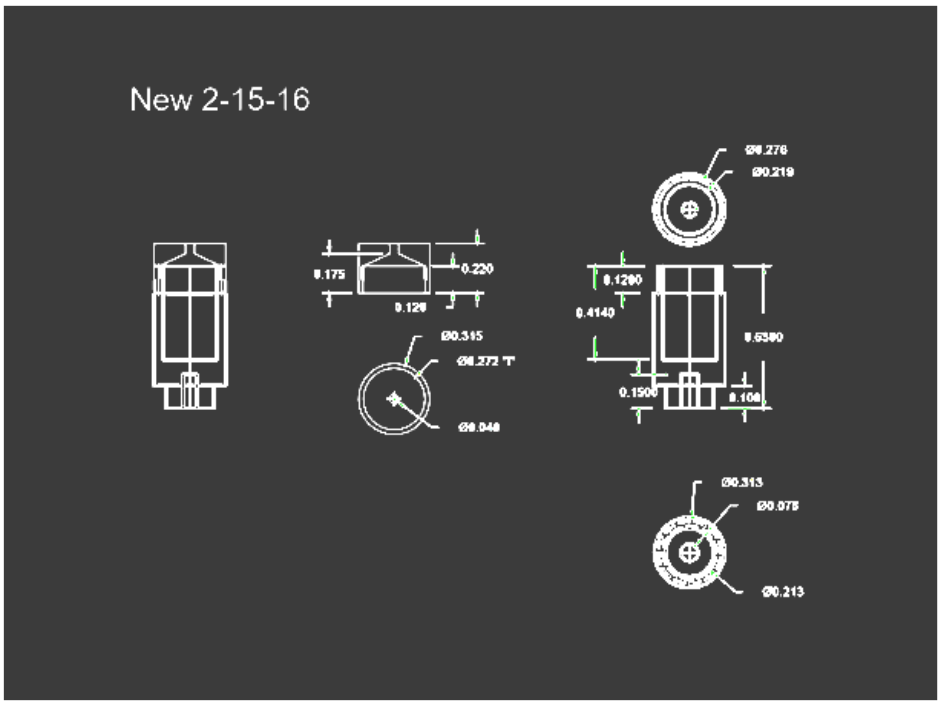

Figure 2. The schematic of the crucible used in the experiments.

Experiment walkthrough

The experiments were prepped prior to the actual experiment. The crucible is cleaned by a sonic bath containing acetone for ten minutes, then dried. The crucible is then placed back into the sonic bath with water and left for 2-3 minutes. It is then dried again and then placed upon a heating plate to set for 25 minutes. At this time, it is picked up by tweezers and placed into a clean container along with the crystal. These are placed into a desiccator overnight. The next day it is taken over to the electronic scale and each piece is weighed. For each experiment, the cap, body, crystal, and overall weight are collected (Table 2). The weight of the basalt powder is then calculated from this procedure. The body of the crucible is filled with basalt powder on the bottom. The olivine crystal is placed upon the bed of the basalt and then the powder is packed around and over the crystal until covered. The cap is placed upon the crucible, and it is placed back in the desiccator. The day before the experiment, the filled crucible was affixed to a

molybdenum rod and mounted into the Knudsen Cell chamber. The chamber is pumped down to 1 x 10^{-8} torr overnight.

After the target pressure is reached, the water-cooling system is turned on to make sure the chamber is cooled. The filament power supply is now turned on and the amperage has increased to 6 Amps to reach a temperature of around 900°C. After this is reached, the high voltage power supply is turned on and used to reach the higher temperatures. The Residual Gas Analyzer (RGA) is used to keep track of the basic gases that are given off during the experiment. When the temperature of the experiment is reached, the temperature, amps, voltage, and pressure were recorded. Each experiment is run for 12 hours. The next day the crucible is taken out of the Knudsen Effusion Cell chamber. The information for each experiment is included in the supplemental table in the appendices.

The crucible will be weighed after the experiment and taken to be cut open, using a heel saw in with a diamond blade. The bottom of the crucibles now shows the crystal and glass that is left from the experiment. This is taken to put into epoxy to analyze. The first epoxy puck contains the 1300° and 1450° crucible experiments, and the second epoxy puck contains the 1600°,1600° (Rhyolite) and 1800° crucible experiments.

Laser ablation inductively coupled plasma mass spectrometer (LA-ICP-MS)

LA-ICP-MS was for trace element analysis. An ESI NWR 193nm Excimer Laser Ablation System was coupled with a Thermo Scientific iCapQ Quadrupole Mass Spectrometer at the University of Arkansas. The crucibles were divided into transects in which spots were created to analyze (Figure 3). The information for the LA-ICP-MS includes: Fluence: 2.6 J/cm^2. Repetition rate: 10 Hz (200 total spots per sample), Gas blank: ~15 seconds, Laser on: 20 seconds, Laser

washout: ~10 seconds, and Gas flow: Helium 0.8 L/min. The reference materials analyzed during the analysis session included San Carlos Olivine (Lambart et al. 2022), BHVO-2 (Raczek et al. 2001), NIST 610, and NIST 612 (Jochum et al. 2012). Data collected from this session was reduced using Iolite with the elements being normalized versus the Calcium concentration in their respective standards. The BHVO-2 points of data provided enough data to be used and showed that the data produced concentrations that were 20% to 30% higher than the published standards. The elements that were taken for the study included: Al, Si, P, K, Sc, Ni, Zn, and Rb.

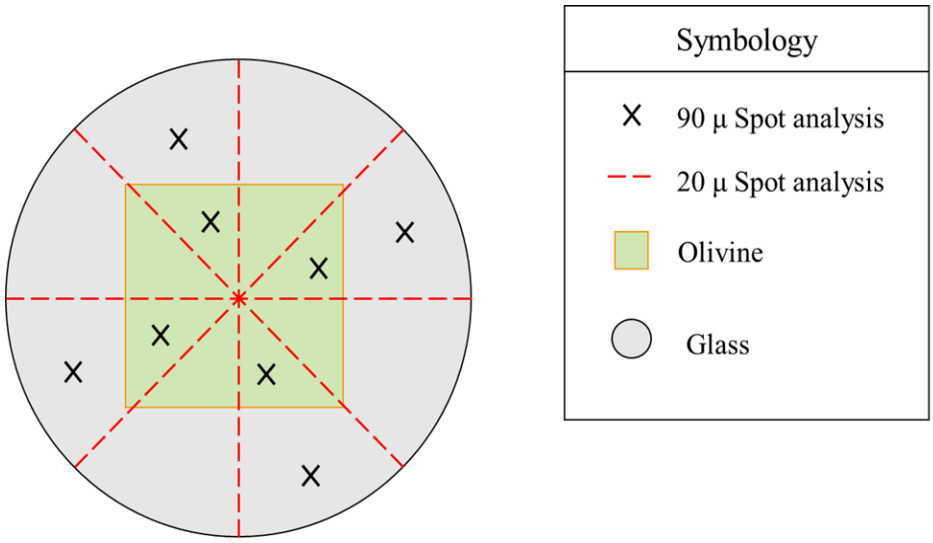

Figure 3. The crucible and crystal layout of the experiment. The dashed lines show the transects that were used to place the 20-micron spots for the LA-ICP-MS.

FEI Quanta 200 SEM

Each experiment was imaged after using a FEI Quanta 200 scanning electron microscope at Missouri State University. Both backscatter electron images and secondary electron images were collected for each experiment sample. These images were used to determine the change in crystal size after the experiment, and to determine locations for in situ trace element and MVE

analysis. Simple pictures were taken of each puck to show the entire area of the crucible (Figure 4 and 5).

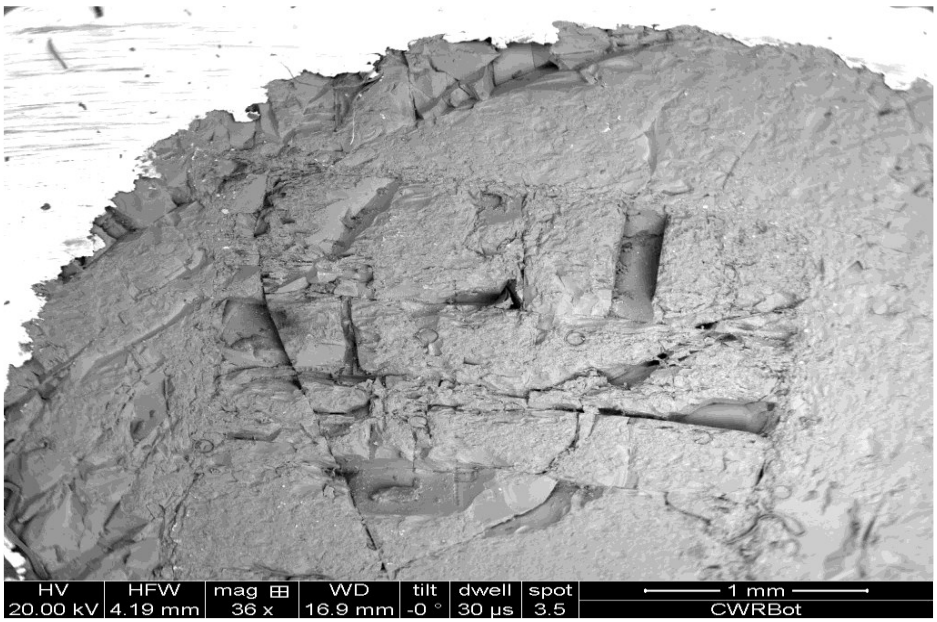

Figure 4. The 1300-degree Celsius top side view of the glass and crystal.

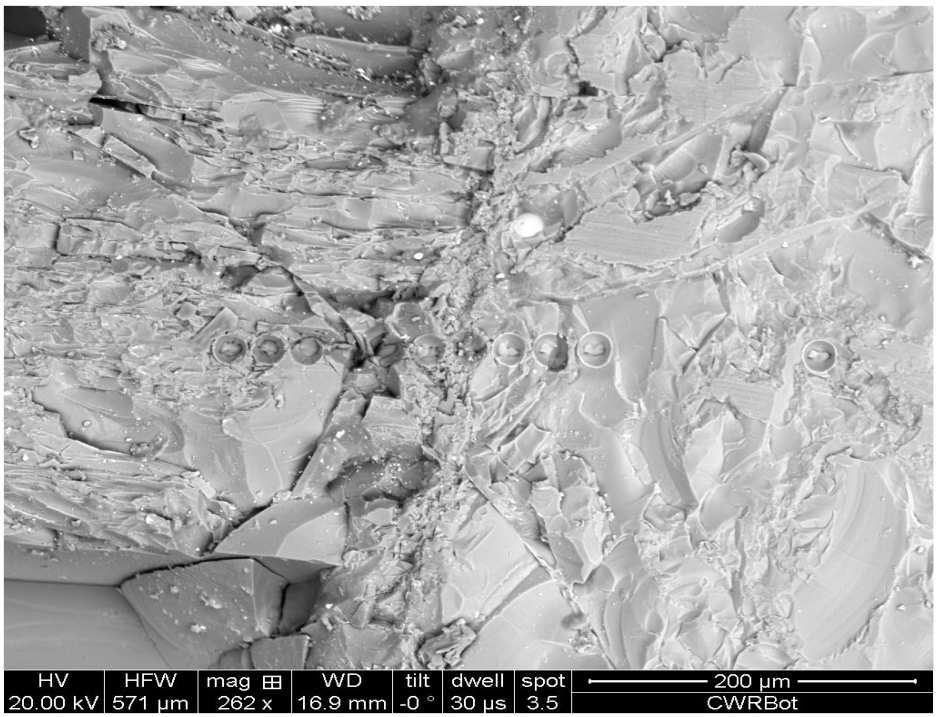

Figure 5. The horizontal transect line around the edge of the crystal into the glass on the right side. The 20-micron pits from the LA-ICP-MS are shown above.

RESULTS

The results from the experiments include individual results from each experiment temperature (Table 4). Data for all experiments were obtained by creating transects which contained roughly forty spots per transect. The spots were spaced out until the glass/olivine boundary was reached and then they were increased to maximize the information. Random points were also collected from the crucible (four from glass and four from olivine). Seven different elements were selected from the range of elements including the three MVEs that are being looked at in his study. The San Carlos olivine analysis produced points that could not be used since they had so many negative values. There were only three that could be used and those showed values that were lower than the standard values for the olivine. The BHVO-2 analysis provided a better value range that could be compared to the standard. The Al, Si, Sc, Ni, and Rb values were within 10-20% of the values of the standard. The values of P, K, and Zn were in a higher concentration range with 20% to 30% higher than that of the standard values. Each element is normalized to SC for direct comparison between the solid and the liquid phases.

1300°C for 12 hours

The diagonal left transect originally had thirty-nine points of data. The data was looked at and reduced due to the information having negatives values which made it conflict with the standard data (Table 3). The points in the glass for the non MVE are Al (71,770 to 83,726 ppm), Sc (35.19 to 37.17 ppm), and Ni (1.58 to 44.98 ppm). The values of the glass for the MVE from the measurement of the LA-ICP-MS are P (186 to 371.6 ppm), K (143 to 947 ppm), Zn (2.07 to

17.9 ppm) and Rb (0.49 to 3.18 ppm). The olivine values for the non-MVE elements are Al (4.6 to 26.35 ppm), Sc (2.10 to 3.48 ppm), and Ni (247 to 644 ppm). The transect non-MVE ranges are Al (4.72 to 64.75 ppm), Sc (1.48 to 1.99 ppm), and Ni (207.46 to 640.7 ppm). These elements values increased towards the middle of the crystal but stay relatively close to the standards. The MVE ranges for the transect are P (107.44 to 157.25 ppm), K (3.50 to 6.83 ppm), Zn (18.2 to 28.56 ppm), and Rb (0.075 to 0.099 ppm). These elements concentrations tended to be small in the middle and larger as you reached the edges of the crystal. Each MVE concentration was normalized to its standard and plotted against another MVE (Figure 6).

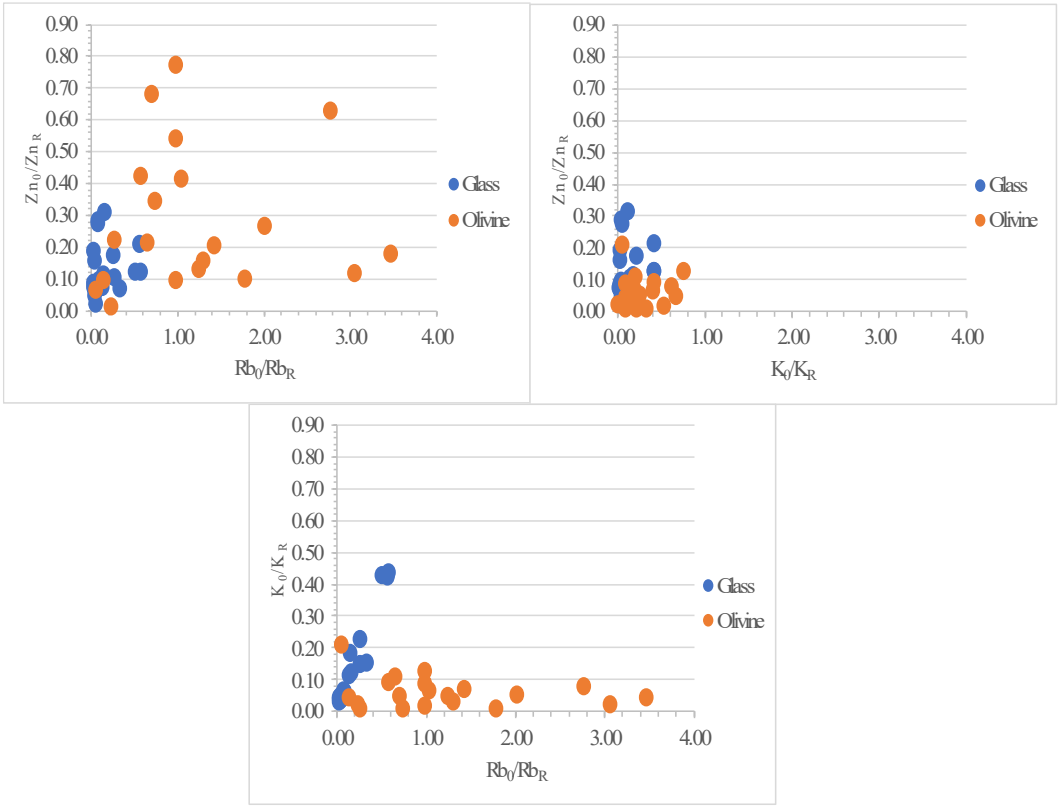

Figure 6. This figure shows the ratio of the measured concentration versus the standard concentration of each MVE plotted against another MVE.

The diagonal right transect originally had thirty-seven points of data and was reduced to 8 points. Points were excluded with values below detection limit. This took the points which could be used down to three points of glass and five points of olivine (Table 3). The points in the glass for the non MVE are Al (73,518 to 75,397 ppm), Sc (34.20 to 36.10 ppm), and Ni (0.002 to 379.27 ppm). The MVE ranges for the transect are P (365.7 to 419.3 ppm), K (108.54 to 163.08 ppm), Zn (7.52 to 19.46 ppm), and Rb (0.30 to 0.351 ppm). The transect non-MVE ranges are Al (3.58 to 781.09 ppm), Sc (0.30 to 3.13 ppm), and Ni (0.01 to 727 ppm). These elements values are higher as you reach the edges of the crystal. The MVE ranges for the transect are P (2.58 to 107.11 ppm), K (8.93 to 44.05 ppm), Zn (0.63 to 36.05 ppm), and Rb (0.033 to 0.347 ppm). The elements value increased from the middle to the edge.

The vertical transect originally had forty-one points of data. This took the points which could be used down to nine points of glass and seven points of olivine (Table 3). The points in the glass for the non-MVE are Al (72,426 to 78,479 ppm), Sc (36.36 to 39.05 ppm), and Ni (0.196 to 28.9 ppm). The MVE ranges for the transect are P (338.88 to 511.75 ppm), K (125.12 to 1841.14 ppm), Zn (4.80 to 29.45 ppm), and Rb (0.396 to 5.42 ppm). The transect non-MVE ranges are Al (9.29 to 1374.44 ppm), Sc (1.04 to 3.45 ppm), and Ni (30.66 to 736.75 ppm). Elemental concentrations increase towards the edge of the glass. The MVE ranges for the transect are P (21.07 to 188.5 ppm), K (13.33 to 102.26 ppm), Zn (3.49 to 40.87 ppm), and Rb (0.0058 to 0.131 ppm). These elemental concentrations trends toward smaller content with spikes before reaching the edges of the crystal. The crystal edges were higher in concentration than the middle.

The horizontal transect originally had forty-one points of data. This took the points which could be used down to three points of glass and five points of olivine (Table 3). The points in the glass for the non MVE are Al (72,426 to 78,479 ppm), Sc (36.36 to 39.05 ppm), and Ni (0.196 to

28.9 ppm); (Figure 8). The MVE ranges for the transect are P (338.88 to 511.75 ppm), K (125.12 to 1841.14 ppm), Zn (4.80 to 29.45 ppm), and Rb (0.396 to 5.42 ppm). The transect non MVE ranges are Al (9.29 to 1374.44 ppm), Sc (1.04 to 3.45 ppm), and Ni (30.66 to 736.75 ppm). These elements values are higher as you reach the edges of the crystal. The MVE ranges for the transect are P (21.07 to 188.5 ppm), K (13.33 to 102.26 ppm), Zn (3.49 to 40.87 ppm), and Rb (0.0058 to 0.131 ppm). The middle of the crystal MVE values were lower than the edges of the crystal with spikes occurring near the edges. All MVE points were plotted with their concentrations and distances (Figure 7).

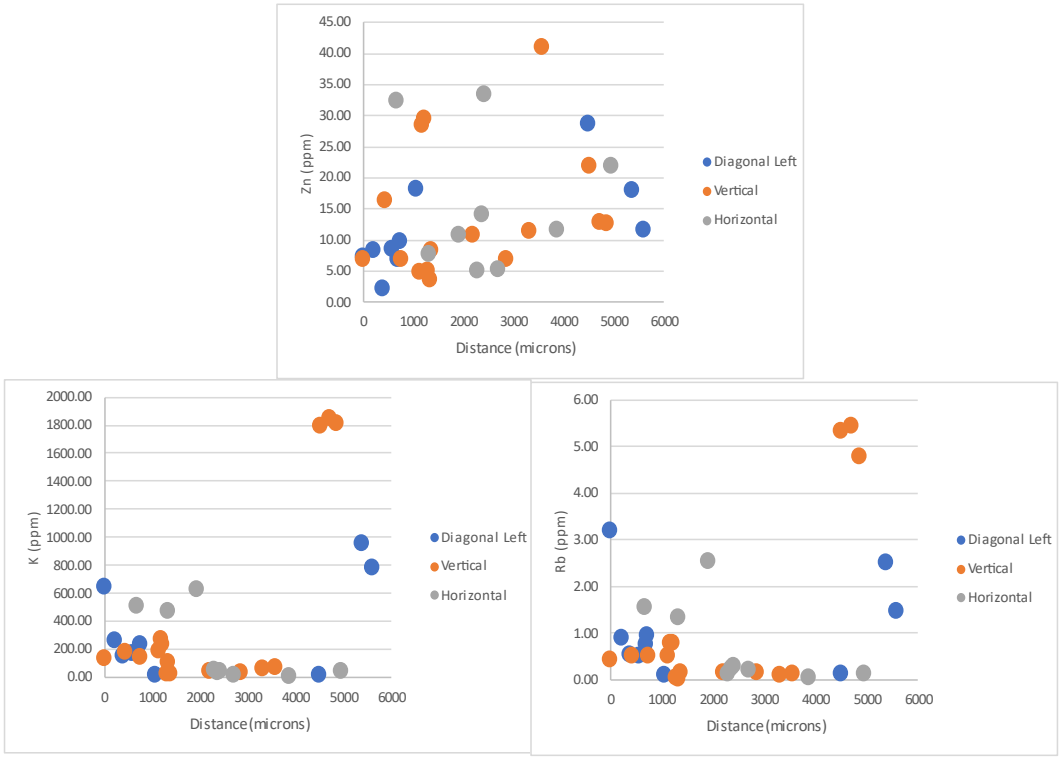

Figure 7. This figure shows the points in relation to their place on the crucible. Three for the transects (DL, V, and H) are shown and the values of the MVE are in ppm.

1450°C for 12 hours

The gas species that were watched during this experiment included hydrogen, carbon dioxide, water, sulfur dioxide, and silicon oxide. The original plan for this experiment was to try for the temperature of 1800°C, but there was hydrogen build up around 1712°C. This prevented the temperature from increasing and the decision was made to make a 1450°C run. The original data had four transect lines that contained 52 spots. The data was analyzed, and it was found that none of the spots could be used due to negative numbers occurring in all the elements. These negative numbers could have been attributed to the laser hitting the tantalum crucible or epoxy. Since there were so many spots having this problem, the run was thrown out.

1600°C for 12 hours

The gas species that were watched during this experiment included hydrogen, carbon dioxide, water, sulfur dioxide, nitrogen, oxygen, and silicon oxide. The original data set contained one-hundred and fifty-eight data points with four transect lines used. The data was analyzed and only sixty-five points remained after deletion of spots. The zinc within the transects seem to peak in the middle of the crucible and at the extreme left and right side. These peaks contain high amounts of zinc (400 ppm left, 15000 ppm middle and 1621 ppm right). The K within the transects of the crucible have three major peaks on the far left and right side and the middle. The peaks contain high amounts of potassium within (1,450 ppm left, 4,350 ppm middle, and 3,950 ppm). The Rb values are also at peaks like Zn and K. The peaks of the Rubidium have the following values within (1.85 ppm left, 22.24 ppm middle, and 14.7 ppm right). The crystal and glass have mixed, and the elements seem to have volatilized and escaped from the outer edges of the crucibles and the middle.

1600°C (Rhyolite) for 12 hours

The gas species that were watched during this experiment included hydrogen, carbon dioxide, water, sulfur dioxide, and oxygen. The original dataset included 93 data points on the four transect lines. After the dataset was analyzed, there were 49 usable data points which were all glass. The aluminum values in these points ranged from 90,000-923,000 ppm. The scandium values of the spots ranged from 8-165 ppm. The three elements that were watched during this study were Zn (0-49 ppm), K (0-535 ppm), and Rb (0-3.34 ppm).

1800°C for 12 hours

The gas species that were watched during this experiment were hydrogen, water, oxygen, sulfur dioxide, silicon oxide, zinc oxide, and nitrogen. There was a previous 1800˚C trial, but that one ended up in eruption due to raising the temperature too fast which increased the pressures of carbon dioxide and water. The second run ended with a dataset which contained one hundred and sixteen datapoints. After further analyzation, all the data points were negative and none of the points could be used. These negative numbers could have been caused by the laser hitting the tantalum or the epoxy. This experiment had to be thrown out due to the lack of information.

DISCUSSION

To fully understand this study, two other studies were used to help guide the parameters. Experiments by Spandler and O'Neill (2010), in which olivine was used as a crucible to house a tetraethyl orthosilicate which was doped with Zn in amounts between 50 micrograms and 1300 micrograms. They then annealed the glass at 1 atm, oxygen fugacity at 10 atm, 1300°C, for different lengths of time. The 2-hour, 24 hour, and 25-day experiments yielded diffusion of zinc into the olivine through cracks in the crystal. This allowed the authors to observe and measure a diffusion coefficient at these constraints.

The second set of experiments were conducted by Neuman et al. (2022). These experiments used the Ortenburg Basalt from Germany and conducted 20 experiments in which they extracted K, Cu, and Zn and created a powder in which they used a furnace at 1 atm, controlling the oxygen fugacity, and heated to different temperatures for different amounts of time. The results showed that there were significant losses in Zn during these experiments that increased with lower oxygen fugacity and more reduced conditions.

The previous two studies show that Zn and other MVEs behave differently under different conditions. The use of performing the studies at atmospheric pressure had differing results due to the preparation of the samples. Neuman et al. (2022) showed that there is a significant loss in MVE elements when exposed to higher temperatures. These conditions were created by extracting the elements from basalt obtained on Earth. The Spandler and O'Neill (2010) study took a natural occurring mineral (olivine) and turned it into a crucible in which a tetraethyl orthosilicate was doped with Zinc and after a few rounds of annealing was placed into the crucible and heated for a significant amount of time which produced diffusion into the olivine crystal. Our study took naturally occurring minerals and rocks from Earth and

created a low-pressure environment which automatically created a low oxygen fugacity. The materials were not altered and placed into a crucible in which were heated to different temperatures to see if diffusion occurred. The results showed that no diffusion occurred from the liquid into the solid, and in fact the concentration of the MVEs significantly decreased in the basalt liquid and the MVEs in the olivine crystal diffused towards the liquid and were eventually lost due to volatilization.

The experiments performed and subsequent analyzation showed that in the glass and olivine non-MVEs stayed within error of the published concentrations of the standard reference materials. The MVE values of the glass, however, are depleted significantly, with K, which is usually around 1150 ppm in BHVO-2, dropping by 50% to 90% of the original concentration (Figure 7). Zinc values in the glass, which usually range between 100 and 150 ppm, have dropped to concentration between 1 to 30 ppm in the glass (Figure 8). The concentrations are lower on the outskirts of the crucible and increase to the edge of the olivine crystal. Rubidium in the glass has the most dramatic drop from 9 ppm to between 0.3 to 3 ppm. The MVEs of the experiment experienced extreme depletion of concentrations in the glass and less in the olivine. The overall trend of these depletion showed that diffusion did not occur from the glass into the olivine, but that diffusion occurred from the olivine into the glass. Those MVEs that diffused then volatilized out of the glass.

The volatilization of the MVEs out of the glass and olivine are shown in Figure 6. This figure shows the measured values of each individual MVE compared to its standard reference concentration of the material it is residing in. Zinc is severely depleted in the glass having lost in the range of 70 to 90% of concentration (Figure 6). In the olivine, the loss isn't as great, but does have loss from anywhere from 20 to 90% of its original concentration (Figure 6). The glass spots are clustered to show that the spots are close in value unlike the olivine spots which are

more spread out. The K and Rb also show clustering in the glass losing anywhere from 60 to 90% of their concentration (Figure 6). The olivine amounts are cluster for K as well, but the other two MVE are spread out a little more though still depleted.

To further show how the depletion occurs over the entire distance of the transect, the concentrations of each MVE were taken and plotted according to their distance from left to right in the crucible and crystal (Figure 7). The overall distance totaled 6000 microns with the crystal making up between the ranges of 1000 to 4000 microns. The Zn graph shows that there is a severe depletion in the glass, but as you look there are spikes in the Zn concentrations which correspond roughly to where the crystal/glass boundary occurs. These spikes occur as well in the K and Rb graphs in which it is also shown that they have severe depletion in the glass in these MVEs.

The graph in Figure 8 takes the spots from all transects with reference to Zn. The spots were split into glass and olivine for the transect and plotted. This graph shows that the overall concentration of Zn in both materials are depleted and in the glass are severely depleted. The overall concentration ranges between 0 and 43 ppm for all spots and that homogeneity doesn't occur (Figure 8). Trendlines were created which show increases in Zn in the olivine as you get closer to the edges of the crystal/glass boundary.

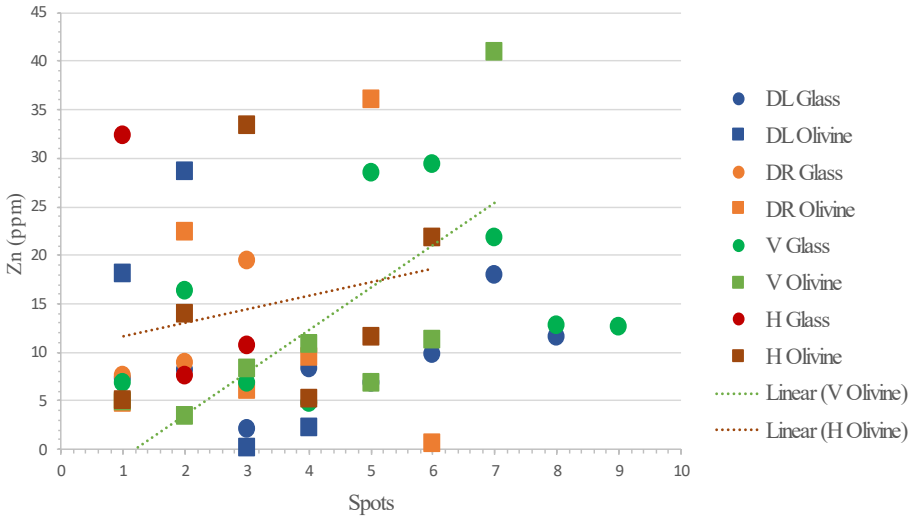

Figure 8. This chart shows the spots from each transect in order from left to right. The concentration of Zn in ppm and trend lines are shown for two of the olivine transect spots.

The overall concentrations of each element analyzed through LA-ICP-MS are shown on a logarithmic scale in Figure 9. This shows that in the glass Al and Sc increases while all the other elements show losses especially the MVE. The bottom graph shows the olivine concentrations of the same elements and in this the elements of Al and P increase while the other elements decrease (Figure 9). The decrease in the olivine is not as severe in the olivine as it was in the glass.

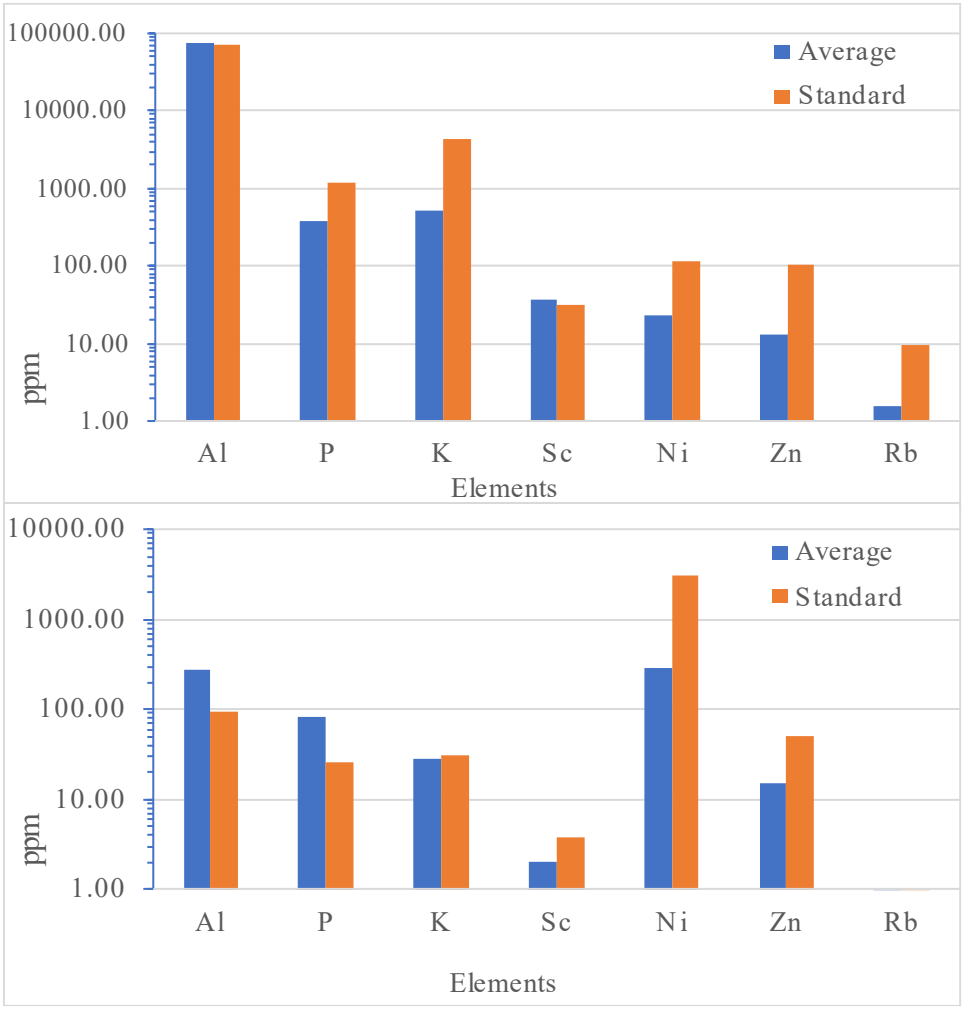

Figure 9. This chart shows the logarithmic scale of the measured values of each element versus the standard value for that element. Glass is shown on the top with olivine on the bottom.

The hypothesis of this study suggested diffusion was a mechanism responsible for the depletion of MVEs in the different types of chondrites. The experiments showed that in less than atmosphere conditions, these MVEs volatilized instead of diffuse. There was diffusion out of the crystal into the liquid, but most of those elements peaked around the edge of the crystal. The transects that were tested showed that the levels of concentration of the MVE were extremely lower than the original levels of the liquid and crystal. There are increases in the levels of some elements like P and Al into the crystal, but these are not MVEs.

CONCLUSION

These experiments were created to identify the mechanism that caused the depletion of Moderately Volatile Elements (MVE) in chondrites that exist in the solar system. There was a single heating event in which everything including elements and molecules were vaporized and then condensed. This created material in which accreted and created items such as chondrules, meteorites, and planetary bodies. The minerals created undergo changes and through the different types of chondrites Moderately Volatile Elements concentrations lower. These concentrations are lower by up to two orders of magnitude. The mechanism that was proposed was diffusion and to check this mechanism an experiment was created through a Knudsen Effusion Cell Chamber. The materials were naturally occurring and heated to temperatures between 1300°C and 1800°C. This study showed the MVE concentration in the crystal diffuse into the liquid resulting in MVE depletion in the crystal. This process led to the concentration around the liquid/crystal border to be higher, but still lower than the original concentration of the crystal. The MVE concentration in the liquid was extremely lower than the original composition. This amount of decrease is suggested to be due to volatilization. Diffusion is suggested to need an atmosphere to occur and more experiments using low pressure and high temperatures are needed. Those experiments will need the same temperatures, which would be held for different lengths shorter than twelve hours and the samples would be larger to make sure there is something to analyze. The crucibles, when placed into epoxy, would need to make sure that the epoxy isn't on the crucibles which means sanding down into the crucible exposing the crystal and glass. This would help in gaining more spots for the LA-ICP-MS to analyze and thus more points to give a clearer answer to this question. For now, the answer to this

mechanism is no when there is little to no pressure, diffusion occurs when under atmospheric pressure with low oxygen fugacity.

The experiments conducted in this study showed that at low pressure and high temperature conditions, diffusion of elements does not occur. The elements volatilize and leave the system even from the solid crystal. For future studies, the crucible used in the study could be changed to an easier metal in which can be cut open easier. The basalt could be doped, but it seems that in doing so that it would still lead to volatilization. Thus, the use of a closed container might help with the volatilization, but the crucible would have to be depressurized to help keep the crucible intact. The use of more basalt might make for better glass and thus more to surround the crystal. The crucibles being placed into the epoxy would have to be monitored and sanded down extremely well to allow for multiple points to be analyzed by an LA-ICP-MS. In this study, many points were created, but few could be used due to the epoxy being in place of glass and crystal.

REFERENCES

Anders E, Ebinhara M (1982) Solar-system abundances of the elements. Geochimica et Cosmochimica Acta 46(11):2363-2380

Anders E, Grevesse N (1989) Abundances of the elements: Meteoritic and solar. Geochimica et Cosmochimica acta 53(1):197-214

Beattie P (1993) Olivine-melt and orthopyroxene-melt equilibria. Contributions to Mineralogy and Petrology 115(1):103-111

Bourdon B, Fitoussi C (2020) Isotope fractionation during condensation and evaporation during planet formation processes. ACS Earth and Space Chemistry 4(8):1408-1423

Chen H, Nguyen BM, Moynier F (2013) Zinc isotopic composition of iron meteorites: Absence of isotopic anomalies and origin of the volatile element depletion. Meteorit. Planet. Sci. 48:2441–2450

Dhaliwal JK, Day JMD, Moynier F (2018) Volatile element loss during planetary magma ocean phases. Icarus 300:249–260

Farcy B, Arevalo R, McDonough WF (2020) K/U of the MORB source and silicate Earth. Journal of Geophysical Research: Solid Earth 125

Greenwood JP, Itoh S, Sakamoto N, Warren P, Taylor L, Yurimoto H (2011) Hydrogen isotope ratios in lunar rocks indicate delivery of cometary water to the Moon. Nature Geosci. 4:79-82

Herzog GF, Moynier F, Albarede F, Berezhnoy AA (2009) Isotopic and elemental abundances of copper and zinc in lunar samples, Zagami, Pele's hairs, and a terrestrial basalt. Geochim. Cosmochim. Acta 73**:**5884**–**5904

Huang J, Zhang X, Chen S, Tang L, Wörner G, Yu H, Huang F (2018) Zinc isotopic systematics of Kamchatka-Aleutian arc magmas controlled by mantle melting, Geochimica et Cosmochimica Acta Volume 238:85-101

Kato C, Moynier F, Valdes MC, Dhaliwal JK, Day J, MD (2015) Extensive volatile loss during formation and differentiation of the Moon. Nat. Commun. 6:7617

Kato C, Moynier F (2017) Gallium isotopic evidence for extensive volatile loss from the Moon during its formation. Science Advances 3(7)

Ku Y, Jacobsen SB (2020) Potassium isotope anomalies in meteorites inherited from the protosolar molecular cloud. Science Advances 6(41)

Labidi J, Cartigny P, Moreira M (2013) Non-chondritic sulphur isotope composition of the terrestrial mantle. Nature 501(7466):208-211

Lambart S, Hamilton S, and Lang OI (2022) Compositional variability of San Carlos olivine. Chemical Geology Volume 605

Larimer JW (1967) Chemical fractionations in meteorites—I. Condensation of the elements. Geochimica et Cosmochimica Acta 31(8):1215-1238

Lodders K, Fegley B (1998) The Planetary Scientist's Companion. Oxford University Press New York

Lodders K (2003) Solar system abundances and condensation temperatures of the elements. The Astrophysical Journal 591(2):1220

Luck J-M, Othman BD, Albarède F, Albarede F (2005) Zn and Cu isotopic variations in chondrites and iron meteorites: Early solar nebula reservoirs and parent-body processes. Geochim. Cosmochim. Acta 69:351–5363

Mahan B, Moynier F, Siebert J, Gueguen B, Agranier A, Pringle EA, Bollard J, Connelly JN and Bizzarro M (2018) Volatile element evolution of chondrules through time. Proceedings of the National Academy of Sciences 115(34):8547-8552

McKenzie DAN, O'nions, RK (1991) Partial melt distributions from inversion of rare earth element concentrations. Journal of petrology 32(5):1021-1091

Moynier F, Albarede F, Herzog G (2006) Isotopic composition of zinc, copper, and iron in lunar samples. Geochim. Cosmochim. Acta 70:6103–6117

Moynier F, Paniello RC, Gounelle M, Albarède F, Beck P, Podosek F, Zanda B (2011) Nature of volatile depletion and genetic relationships in enstatite chondrites and aubrites inferred from Zn isotopes. Geochim. Cosmochim. Acta 75:297–307

Moynier F, Vance D, Fujii T, Savage P (2017) The Isotope Geochemistry of Zinc and Copper. Rev. Mineral. Geochemistry 82:543–600

NASA (2022) NASA Strategic Plan, 2022, https://www.nasa.gov/sites/default/files/atoms/files/2022_nasa_strategic_plan.pdf

Neuman M, Holzheid A, Lodders K, Fegley Jr B, Jolliff BL, Koefoed P, Chen H Wang K (2022) High temperature evaporation and isotopic fractionation of K and Cu. Geochimica et cosmochimica acta 316:1-20

Nebel O, Mezger K, van Westrenen W (2011) Rubidium isotopes in primitive chondrites: Constraints on Earth's volatile element depletion and lead isotope evolution. Earth and Planetary Science Letters 305(3–4):309-316

Norris CA Wood BJ (2017) Earth's volatile contents established by melting and vaporization. Nature 549(7673):507-510

O'Neill HSC, Palme H (2008) Collisional erosion and the non-chondritic composition of the terrestrial planets. Philosophical Transactions of the Royal Society A: Mathematical, Physical and Engineering Sciences 366(1883):4205-4238

Palme H, Larimer JW Lipschutz ME (1988) Moderately volatile elements. Meteorites and the early solar system. 436-461

Paniello RC, Day JM Moynier F (2012) Zinc isotopic evidence for the origin of the Moon. Nature 490(7420):376-379

Pringle EA Moynier F (2017) Rubidium isotopic composition of the Earth, meteorites, and the Moon: Evidence for the origin of volatile loss during planetary accretion. Earth and Planetary Science Letters 473:62-70

Prior GT (1920) The classification of Meteorites. Mineralogical magazine and journal of the Mineralogical Society 19(90):51-63

Raczek Ingrid, Stoll B, Hofmann, Albrecht, Jochum Klaus (2001) High-precision trace element data for the USGS reference materials BCR-1, BCR-2, BHVO-1, BHVO-2, AGV-1, AGV-2, DTS-1, DTS-2, GSP-1 and GSP-2 by ID-TIMS and MIC-SSMS. Geostandards Newsletter 25:77-86

Sharp ZD, Shearer CK, McKeegan KD, Barnes JD, Wang YQ (2010) The chlorine isotope composition of the Moon and implications for an anhydrous mantle. Science 329(5995):1050-1053

Shearer CK, Hess PC, Wieczorek MA, Pritchard ME, Parmentier EM, Borg LE, Longhi J, Elkins-Tanton LT, Neal CR, Antonenko I, Canup RM (2006) Thermal and magmatic evolution of the Moon. Reviews in Mineralogy and Geochemistry 60(1):365-518

Siebert J, Shahar A (2015) An experimental geochemistry perspective on Earth's core formation. The early Earth: accretion and differentiation 103-121

Sossi PA, Nebel O, O'Neill HSC Moynier F (2018) Zinc isotope composition of the Earth and its behaviour during planetary accretion. Chemical Geology 477:73-84

Spandler C, O'Neill HSC (2010) Diffusion and partition coefficients of minor and trace elements in San Carlos olivine at 1,300 C with some geochemical implications. Contributions to Mineralogy and Petrology 159:791-818

Tera F, Eugster O, Burnett DS Wasserburg GJ (1970) Comparative study of Li, Na, K, Rb, Cs, Ca, Sr, and Ba abundances in achondrites and in Apollo 11 lunar samples. In Geochimica et Cosmochimica Acta Supplement Volume 1. Proceedings of the Apollo 11 Lunar Science Conference held 5-8 January 1970 in Houston, TX. Volume 2: Chemical and Isotope Analyses

Wang K, Jacobsen SB (2016) An estimate of the Bulk Silicate Earth potassium isotopic composition based on MC-ICPMS measurements of basalts. Geochim. Cosmochim. Acta 178:223–232

Wood BJ, Walter MJ, Wade J (2006) Accretion of the Earth and segregation of its core. Nature 441(7095):825-833

Zeng H, Rozsa VF, Nie NX, Zhang Z, Pham TA, Galli G, Dauphas N (2019) Ab Initio Calculation of Equilibrium Isotopic Fractionations of Potassium and Rubidium in Minerals and Water. ACS Earth Sp. Chem. 3:2601–2612

Zhang ZJ, Nie NX, Mendybaev RA, Liu MC, Hu JJ, Hopp T, Alp EE, Lavina B, Bullock ES, McKeegan KD Dauphas N (2021) Loss and isotopic fractionation of alkali elements during diffusion-limited evaporation from molten silicate: Theory and experiments. ACS Earth and Space Chemistry 5(4):755-784

TABLES

Table 1. The Standard Reference concentrations for each element in the study.

Standards	^{27}Al ppm	^{29}Si ppm	^{31}P ppm	^{39}K ppm	^{45}Sc ppm	^{60}Ni ppm	^{66}Zn ppm	^{85}Rb ppm
San Carlos	94	186986	26	31.29	3.81	3045	50	0.001
BHVO-2	71600	233000	1200	4300	32	119	103	9.8

Table 2. This table shows the weights of the parts of the crucible along with its contents.

Crucible Chart (Weights in grams)							
Thesis Experiments							
12 hours							
	1000 C	1300 C	1600 C	1800 C	1450 C	1600 C (RHY)	1800 C
Lid	2.9066	2.2855	2.9032	1.8598	2.1736	2.1285	1.6814
Container	7.1556	7.0462	7.1885	7.2789	6.9183	7.2019	7.138
Crystal	0.0568	0.0865	0.0944	0.0608	0.0788	0.0661	0.0549
Basalt	0.078	0.1474	0.1505	0.1509	0.1505	0.0868	0.1509
Before	10.197	9.5656	10.3366	9.3504	9.3212	9.4833	9.0252
After	10.197	9.5570	10.2473	eruption	9.2010	9.3930	8.5138

Table 3. This table shows the points of the experiment in which the LA-ICP-MS analyzed and found concentrations.

Name	Type	^{27}Al ppm	^{29}Si ppm	^{31}P ppm	^{39}K ppm	^{45}Sc ppm	^{60}Ni ppm	^{66}Zn ppm	^{85}Rb ppm
CW1.TOPDL.01	Glass	78199.78	264997.23	335.66	636.90	36.52	2.96	7.27	3.18
CW1.TOPDL.02	Glass	78269.18	251393.84	357.64	252.81	36.62	3.01	8.23	0.87
CW1.TOPDL.03	Glass	78121.67	252352.93	342.02	143.85	36.18	1.59	2.07	0.52
CW1.TOPDL.04	Glass	78085.97	259075.20	371.67	159.55	37.17	14.89	8.40	0.49
CW1.TOPDL.05	Glass	75903.58	246141.85	310.26	164.86	36.19	1.88	6.78	0.74
CW1.TOPDL.06	Glass	71770.16	247089.07	296.30	226.54	35.64	44.98	9.76	0.91
CW1.TOPDL.38	Glass	79852.85	252581.76	186.72	947.94	36.37	9.15	17.95	2.48
CW1.TOPDL.39	Glass	83726.93	264681.74	208.25	770.86	35.19	1.85	11.57	1.44
CW1.TOPDR.01	Glass	73518.90	254782.94	365.74	108.54	34.20	0.00	7.52	0.35
CW1.TOPDR.02	Glass	75397.71	267109.29	419.33	159.21	36.11	6.65	8.88	0.33
CW1.TOPDR.03	Glass	75278.21	254082.51	409.11	163.08	35.09	379.28	19.47	0.30
CW1-TOP.V.01	Glass	75846.49	257101.87	406.80	125.12	36.92	1.16	6.92	0.40
CW1-TOP.V.02	Glass	78119.94	278543.24	511.75	170.32	39.05	28.91	16.30	0.49
CW1-TOP.V.03	Glass	75667.84	260964.44	458.19	139.43	38.04	0.20	6.85	0.48
CW1-TOP.V.04	Glass	75389.04	264669.61	436.97	183.50	37.61	1.11	4.80	0.48
CW1-TOP.V.05	Glass	74242.97	255593.15	436.64	261.20	37.31	20.53	28.45	0.76
CW1-TOP.V.06	Glass	72426.93	254207.23	442.39	222.01	38.45	2.40	29.45	0.76
CW1-TOP.V.38	Glass	75063.09	255276.30	338.88	1790.27	37.39	0.39	21.88	5.31
CW1-TOP.V.39	Glass	78479.31	256170.20	364.77	1841.14	36.81	0.40	12.72	5.42
CW1-TOP.V.40	Glass	76144.12	248881.77	386.61	1809.83	36.36	5.15	12.66	4.76
CW1 TOP.H.01	Glass	78295.46	279053.36	504.12	502.87	34.80	3.67	32.29	1.52
CW1 TOP.H.02	Glass	76494.30	264613.32	444.63	467.53	36.77	0.28	7.64	1.31
CW1 TOP.H.03	Glass	75219.76	259576.91	382.00	620.64	38.24	2.95	10.68	2.52
CW1.TOPDL.12	Olivine	12.94	36013.41	157.25	3.50	1.69	404.22	18.18	0.07
CW1.TOPDL.28	Olivine	64.75	44662.76	107.44	6.83	1.99	640.71	28.57	0.10
CW1.TOPDR.20	Olivine	33.41	21395.29	71.98	44.05	0.66	261.41	22.46	0.06
CW1.TOPDR.26	Olivine	3.59	2838.95	3.53	8.93	0.75	47.79	6.07	0.31
CW1.TOPDR.33	Olivine	5.37	14726.21	59.76	19.60	0.30	197.64	9.53	0.35
CW1.TOPDR.36	Olivine	73.46	48730.65	107.12	22.65	3.13	727.49	36.06	0.07
CW1.TOPDR.37	Olivine	781.09	2917.47	5.11	9.40	0.34	0.01	0.63	0.02
CW1-TOP.V.07	Olivine	1374.44	41547.26	79.90	19.57	3.03	156.34	4.91	0.01
CW1-TOP.V.08	Olivine	371.00	47838.28	188.50	102.26	3.46	736.75	3.49	0.01
CW1-TOP.V.09	Olivine	93.48	11135.16	35.51	13.33	1.04	33.17	8.26	0.13
CW1-TOP.V.15	Olivine	43.86	11143.93	21.07	34.24	2.17	30.66	10.80	0.14
CW1-TOP.V.18	Olivine	9.29	21085.40	73.18	21.36	1.85	231.73	6.80	0.13
CW1-TOP.V.20	Olivine	12.47	12161.45	92.27	52.60	1.22	215.88	11.36	0.07
CW1-TOP.V.22	Olivine	741.55	27720.23	48.90	61.32	1.63	346.92	40.88	0.10
CW1 TOP.H.04	Olivine	1890.23	77713.47	100.43	42.49	5.99	167.80	5.06	0.10
CW1 TOP.H.06	Olivine	11.32	18099.71	43.97	24.70	4.22	306.03	13.99	0.20
CW1 TOP.H.07	Olivine	19.18	37630.90	133.35	37.36	2.89	550.10	33.36	0.28
CW1 TOP.H.09	Olivine	5.56	2706.87	-20.18	3.40	2.30	55.35	5.26	0.18
CW1 TOP.H.33	Olivine	0.45	5705.02	117.31	2.63	0.07	112.76	11.64	0.03
CW1 TOP.H.34	Olivine	10.44	36015.77	157.25	30.08	0.99	530.29	21.88	0.10

Table 4. This table shows the times, temperatures, pressure, amps, and watts of the experiments.

Experiment (1300 °C)					
Time (min)	Temperature (°C)	Pressure (torr)	Amps	Voltage	Power (watt)
12:00	1313	1.73E-07	0.11	380	41.8
13:00	1310	1.23E-07	0.11	370	40.7
14:00	1296	1.11E-07	0.106	370	39.22
15:00	1295	1.07E-07	0.095	420	39.9
16:00	1298	9.97E-08	0.093	430	39.99
17:00	1296	9.49E-08	0.092	440	40.48
18:00	1301	8.96E-08	0.092	440	40.48
19:00	1298	8.61E-08	0.091	440	40.04
20:00	1295	8.33E-08	0.091	440	40.04
21:00	1298	8.01E-08	0.09	450	40.5
22:00	1297	7.72E-08	0.09	450	40.5
23:00	1295	7.47E-08	0.09	450	40.5
0:00	1294	7.23E-08	0.09	450	40.5
Experiment (1450 °C)					
7:34	1453	2.52E-07	0.122	510	62.22
8:34	1634	2.53E-07	0.146	1020	148.92
9:34	1547	2.03E-07	0.145	1060	153.7
10:34	1458	1.48E-07	0.135	900	121.5
11:34	1467	1.55E-07	0.135	890	120.15
12:34	1457	1.61E-07	0.132	870	114.84
13:34	1463	1.58E-07	0.132	870	114.84
14:34	1462	1.55E-07	0.132	870	114.84
15:34	1464	1.52E-07	0.132	860	113.52
16:34	1449	1.49E-07	0.132	860	113.52
17:34	1445	1.46E-07	0.132	860	113.52
18:34	1442	1.42E-07	0.132	860	113.52
19:34	1448	1.38E-07	0.133	860	114.38
Experiment (1600 °C)					
10:00	1600	1.66E-07	0.125	770	96.25
11:00	1607	1.39E-07	0.117	830	97.11
12:00	1613	2.13E-07	0.12	830	99.6
13:00	1604	2.05E-07	0.121	830	100.43
14:00	1598	1.87E-07	0.121	830	100.43
15:00	1596	1.79E-07	0.12	830	99.6
16:00	1599	1.71E-07	0.12	840	100.8
17:00	1599	1.64E-07	0.12	840	100.8
18:00	1601	1.59E-07	0.12	840	100.8
19:00	1601	1.55E-07	0.12	840	100.8
20:00	1601	1.51E-07	0.119	840	99.96
21:00	1600	1.47E-07	0.119	840	99.96
22:00	1601	1.42E-07	0.119	840	99.96
Experiment (1600 °C) Rhyolite					
12:00	1601	5.35E-08	0.15	830	124.5
13:00	1589	1.24E-07	0.15	720	108
14:00	1578	1..23E-07	0.15	710	106.5
15:00	1570	8.02E-08	0.15	700	105
16:00	1565	7.00E-08	0.15	690	103.5
17:00	1563	6.40E-08	0.15	690	103.5
18:00	1560	6.18E-08	0.15	680	102
19:00	1558	5.90E-08	0.15	680	102
20:00	1556	5.54E-08	0.15	680	102
21:00	1554	5.21E-08	0.15	680	102
22:00	1553	5.02E-08	0.15	680	102
23:00	1552	4.83E-08	0.15	680	102
0:00	1550	4.65E-08	0.15	680	102
Experiment (1800 °C)					
9:24	1750	2.66E-07	0.175	1400	245.00
10:24	1797	7.84E-07	0.175	1480	259.00
11:24	1777	5.93E-07	0.169	1480	250.12
12:24	1826	6.08E-08	0.176	1490	262.24
13:24	1816	5.26E-08	0.197	1180	232.46
14:24	1810	5.13E-08	0.203	1100	223.30
15:24	1819	5.13E-08	0.203	1100	223.30
16:24	1813	5.11E-08	0.203	1080	219.24
17:24	1812	5.10E-08	0.201	1080	217.08
18:24	1809	5.10E-08	0.2	1080	216.00
19:24	1806	5.03E-08	0.198	1080	213.84
20:24	1801	4.93E-08	0.196	1080	211.68
21:24	1807	4.92E-08	0.196	1100	215.60